Available online at www.sciencedirect.com
ScienceDirect
Trans. Nonferrous Met. Soc. China 22(2012) 2098−2105
Transactions of Nonferrous Metals Society of China
www.tnmsc.cn

Kinetics and microstructural evolution during recrystallization of a Ni_3Al-based single crystal superalloy

WU Yu-xiao[1], ZHANG Heng[1], LI Fu-lin[1], LI Shu-suo[1, 2], GONG Sheng-kai[1, 2], HAN Ya-fang[1, 3]

1. School of Materials Science and Engineering, Beihang University, Beijing 100191, China;
2. Key Laboratory of Aerospace Materials and Performance (Ministry of Education), Beihang University, Beijing 100191, China;
3. Beijing Institute of Aeronautical Materials, Beijing 100095, China

Received 21 November 2011; accepted 15 March 2012

Abstract: The recrystallization kinetics and microstructural evolution of a Ni_3Al-based single crystal superalloy were presented, especially the different recrystallization behaviors between the dendrite arm and the interdendritic region. The single crystal alloy was deformed by grit blasting. A succeeding annealing under inert atmosphere at 1280 °C for different time led to the formation of recrystallized grains close to the grit blasting surface. It was found that the recrystallization depth and velocity in the dendrite arm were respectively deeper and faster than those in the interdendritic region where the Y-NiMo phase existed. The recrystallization process in the interdendritic region was significantly inhibited by the Y-NiMo precipitates. However, the pinning effect gradually weakened with the annealing time due to the dissolution of the Y-NiMo phase, and the recrystallization depth in the dendrite arm was deeper than that in the interdendritic region.

Key words: recrystallization; kinetics; Y-NiMo phase; Ni_3Al based single crystal superalloy

1 Introduction

Single crystal superalloys possess important applications in gas turbine blades and vanes due to their excellent elevated temperature mechanical properties compared with polycrystalline materials. Nevertheless, strain-induced recrystallization (RX) is a well-known problem in the production and service of the single crystal alloy parts. It is known that a certain volume of recrystallization may dramatically reduce their creep rupture strength [1,2] and fatigue life [3,4]. During manufacturing and processing of the new parts, plastic deformation might be induced by shell removal, stamping identification and grit blasting [5]. Subsequently, surface recrystallization may take place during the solution treatment, which can introduce disadvantageous orientations and high-angle grain boundaries.

To solve this problem, the recrystallization behaviors of nickel-based single crystal superalloys such as SRR99 [6], CMSX-2 [7] and CMSX-4 [8] have been studied. However, the recrystallization behavior of the Ni_3Al-based single crystal superalloys is not yet clear [9,10]. LI et al [10] mainly studied the cellular microstructure which transformed by large γ' particles during recrystallization of a Ni_3Al-based single crystal superalloy, IC6SX. BAKER et al [11] investigated the recrystallization kinetics of cold-rolled Ni_3Al, whereas a deep insight on the recrystallization kinetics and microstructural evolution of the Ni_3Al-based single crystal alloy is not presented. In addition, recrystallization kinetics in the dendrite arm and interdendritic region has been rarely reported.

Ni_3Al is one of the most extensively studied intermetallic compounds and a variety of Ni_3Al-based materials have been developed for elevated temperature applications [12−14]. To meet the ever-increasing demand for higher operating temperatures in the aeroengine, a new Ni_3Al-based superalloy, IC21, has been recently developed which exhibits excellent high temperature mechanical properties. Systematic analysis of recrystallization behavior of IC21 has been limited. Thus, a detailed study of recrystallization kinetics and

Foundation item: Project (50971005) supported by the National Natural Science Foundation of China
Corresponding authors: GONG Sheng-kai; Tel: +86-10-82339003; E-mail: gongsk@buaa.edu.cn;
LI Shu-suo; Tel: +86-10-82314488; E-mail: lishs@buaa.edu.cn
DOI: 10.1016/S1003-6326(11)61434-9

microstructural evolution of IC21was carried out. Efforts were also made to understand the role of Y-NiMo phase which made a difference on the recrystallization behavior between the dendrite arm and the interdendritic region.

2 Experimental

A Ni_3Al-based single crystal superalloy, IC21, was used in the present study with the nominal composition of Ni−(8−9)Al−(10−13)Mo−(1−2)Re (mass fraction, %). The master alloy was firstly prepared by a vacuum induction furnace, and then the single crystal alloy was produced in the <001> direction by screw crystal selection method in a DZG−0.025 directionally solidified furnace. The as-prepared alloy was cut into small pieces of 15 mm × 10 mm × 3 mm (with 15 mm × 10 mm face parallel to growth direction), mechanically ground and polished, and then grit blasted by Al_2O_3 balls for 1 min at 0.40 MPa. The deformed samples were encapsulated in a quartz tube under argon atmosphere, and annealed at 1280 °C for 10, 30, 60, 120, 240, 600 and 1200 min, respectively, then followed by air cooling. Samples for internal recrystallization observation were cut along the cross-section of recrystallized surface by an electric discharge machine.

The microstructures of the specimens were characterized by an optical microscope and Apollo 300 scanning electron microscope (BSEI) equipped with energy dispersive X-ray spectrum (EDS). The chemical compositions of the phases and element segregation were determined by JXA−8100 electron probe micro-analyzer (EPMA). The overall average recrystallization depth, the average depth both in the dendrite arm and the interdendritic region were measured from at least eight optical metallographs for each sample. Microhardness values were obtained by a Vickers hardness testing machine (HXZ−1000).

3 Results and discussion

3.1 As-cast microstructure

The as-cast microstructure of the alloy presented in Fig. 1(a) exhibited a typical dendritic structure with the primary dendritic arm spacing of about 400 μm. There were three phases in this alloy illustrated in Fig. 1(b). The dark phase was γ'-Ni_3Al (Mo, Re), the grey phase with a skeletal network around γ' phase was γ-Ni (Mo, Re) and the white phase with irregular, and strip or block morphologies, whose chemical composition was 6.68Al−44.21Ni−46.72Mo−2.40Re (mole fraction, %) obtained by EPMA, was identified as primary Y-NiMo phase [15−17]. The as-cast microstructure of the single-crystal alloy can be divided into interdendritic region (IR) and dendrite arm (DA), as shown in Fig. 1(b). The interdendritic region consisted of fine γ' precipitates with the size of 0.5−1.0 μm, whereas the γ' precipitates in the dendrite arm was coarse and the size was 1.0−5.5 μm.

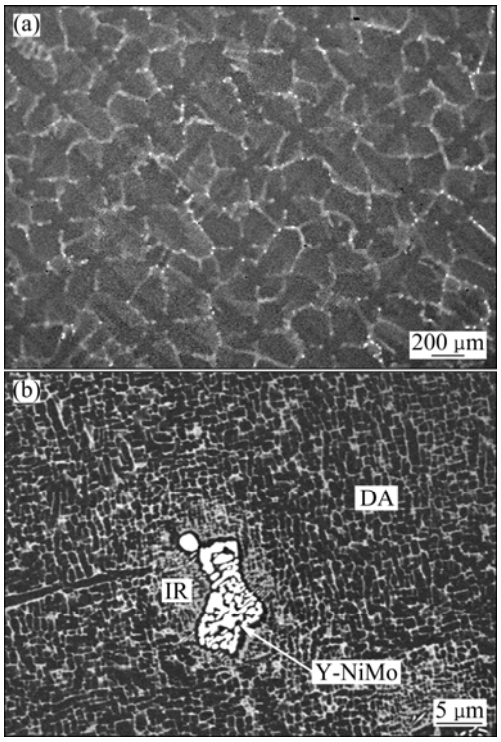

Fig. 1 BSE images of as-cast single crystal superalloy: (a) Dendritic structure; (b) Enlargement of circular area in (a) showing dendrite arm and interdendritic region

The elements contents of the interdendrite and dendrite regions were determined by EPMA, as illustrated in Table 1. Based on the EPMA results, the element segregation coefficient, k, defined as the element contents of the interdendrite and dendrite, was obtained and also listed in Table 1. Obviously, the γ' phase forming element Al mainly partitioned into the dendrite arm. However, element Mo tended to be enriched in the interdendritic region since Mo mainly entered in the γ phase. Re distributed in both regions with a slightly higher content in the interdendritic region. The results were consistent with the BSE image in Fig. 1(b).

Table 1 Element contents and element segregation coefficient (k) in interdendritic region and dendrite arms

Element	w/%		
	Interdendrite	Dendrite	k
Al	6.18	8.29	0.75
Ni	68.91	76.56	0.90
Mo	23.11	13.63	1.70
Re	1.80	1.52	1.18

The microstructure underneath the surface after grit blasting was severely tortured, as illustrated in Fig. 2(a). It was found that grit blasting caused work hardening of the surface layers by means of a microhardness traverse with applying 4.9 N load for 10 s. The microhardness profile below the surface of the grit blasted material was illustrated in Fig. 2(b), where it may be seen that a cold worked layer with depth of 100 μm was present. In addition, the plastic deformation weakened as the distance was gradually further away from the surface of the sample. It is considered that the free energy of the single crystal alloy was raised during deformation due to the presence of dislocations and point defects, in other words, the deformed material containing these defects was thermodynamically unstable. Subsequently, the deformed region would provide the driving force for nucleation and growth of the new grains during annealing.

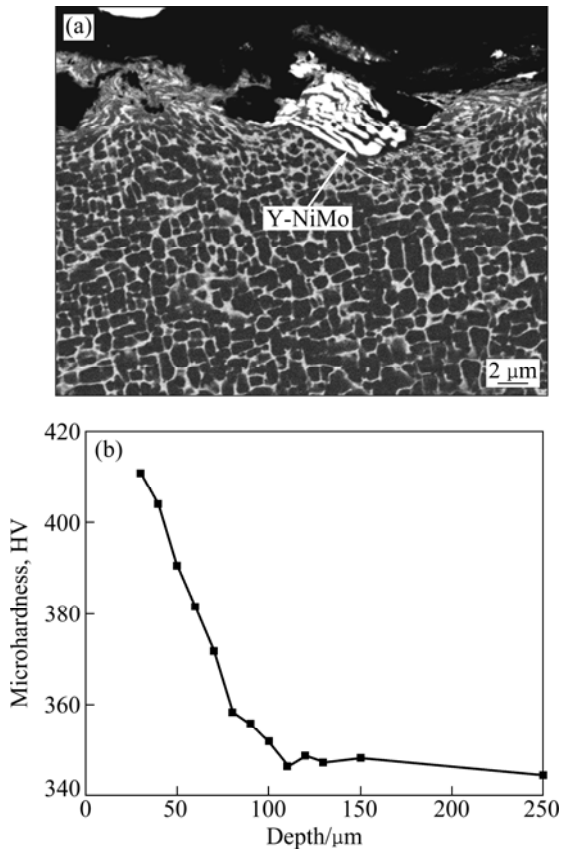

Fig. 2 BSE image showing microstructure of as-cast single crystal superalloy after grit blasting (a) and microhardness profile below grit blasted surface (b)

3.2 Recrystallization kinetics

In this part, the recrystallization kinetics has been studied by examining the microstructure variations of the samples which were annealed at 1280 °C for different time after grist blasting. The recrystallization layer formed after annealing with the depth of recrystallization shown in Fig. 3(a). The relationship between the annealing time and the recrystallization depth of the whole sample, the dendrite arm and the interdendritic region is illustrated in Fig. 3(b). It is seen that the development of recrystallization was very fast within the first 60 min and gradually slowed down with the isothermal time. This tendency was consistent with previous literatures [6,18]. However, recrystallization kinetics in the dendrite arm was different from that in the interdendritic region. Not only was the recrystallization depth in the dendrite arm deeper than in the interdendritic region, but also the recrystallization velocity was faster, as indicated in Fig. 3(b). It has been reported that the migration of recrystallization can be pinned by undissolved γ' phase [6,18]. While most of the γ' phase dissolved at 1280 °C in the present investigation, thus the advancing front of recrystallized grains would not be retarded by γ' phase heavily. In addition, the size of γ' phase in the dendrite arm was larger than that in the interdendritic region and consequently more hardly dissolved. Therefore, γ' phase was not the key factor which may lead to the difference in the recrystallization kinetics between the two regions.

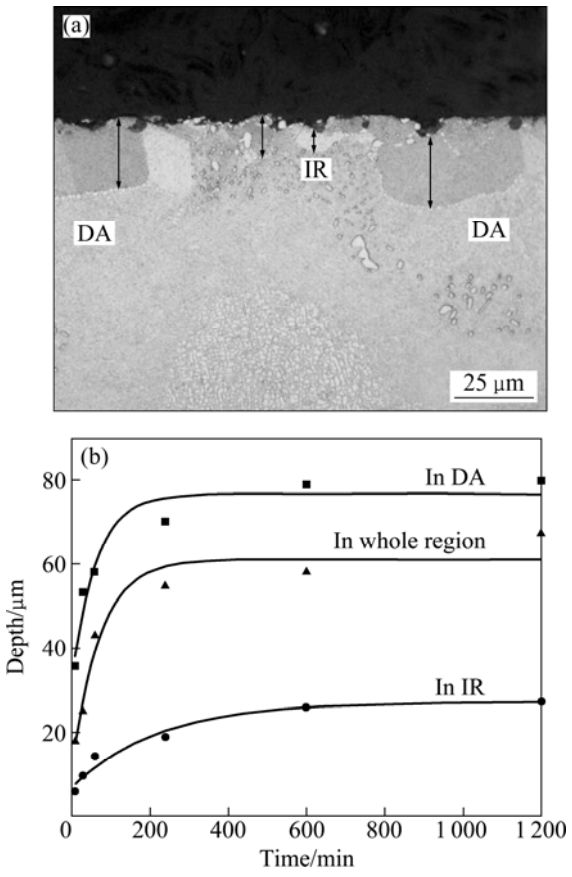

Fig. 3 BSE image illustrating depth of recrystallization layer (a) and relationship between average recrystallization depth and annealing time at 1280 °C (b)

3.3 Microstructural evolution

As discussed above, γ' phase was not the factor which may lead to the different recrystallization kinetics between the dendrite arm and the interdendritic region. In order to make clear the reason which accounted for it, the microstructural evolution of the samples close to the grit blasting surface was studied, as shown in Fig. 4. It can be seen that the recrystallization behavior in the dendrite arm was quite different from that in the interdendritic region where there were the white precipitates. Obviously, the recrystallization depth grew faster in the dendrite arm than that in the interdendritic region. This agreed well with that seen in Fig. 3. In the interdendritic region, a large amount of white phase with needle, granule, short rod and bulk shapes was observed in Fig. 4(a) and the amount became more (Fig. 4(b)), then reduced greatly (Figs. 4(c)−(f)). Meanwhile, the recrystallization was severely inhibited by the white precipitates in the interdendritic region, but they did not retard the advancing front of the recrystallized grains after 10 h, as shown in Figs. 4(e) and (f) in contrast with Figs. 4(a)−(d).

Figure 5 shows the microstructural morphologies of the matrix further away from the grit blasting surface. From the as-cast microstructure, it was known that the primary Y-NiMo phase with irregular, and strip or block morphologies existed in the interdendritic region. Figure 5 suggested that the primary Y-NiMo phase gradually dissolved into the matrix. When the sample was annealed at 1280 °C for 1200 min, this phase completely disappeared. Obviously, the microstructural morphologies of the matrix were quite different from those close to the grit blasting surface which would be discussed subsequently.

Firstly, the identification of the white precipitates with needle, granule and short rod shapes in Fig. 4(a) was carried out. Compared with Fig. 5(a), the white phase with bulk shape in Fig. 4(a) was the primary

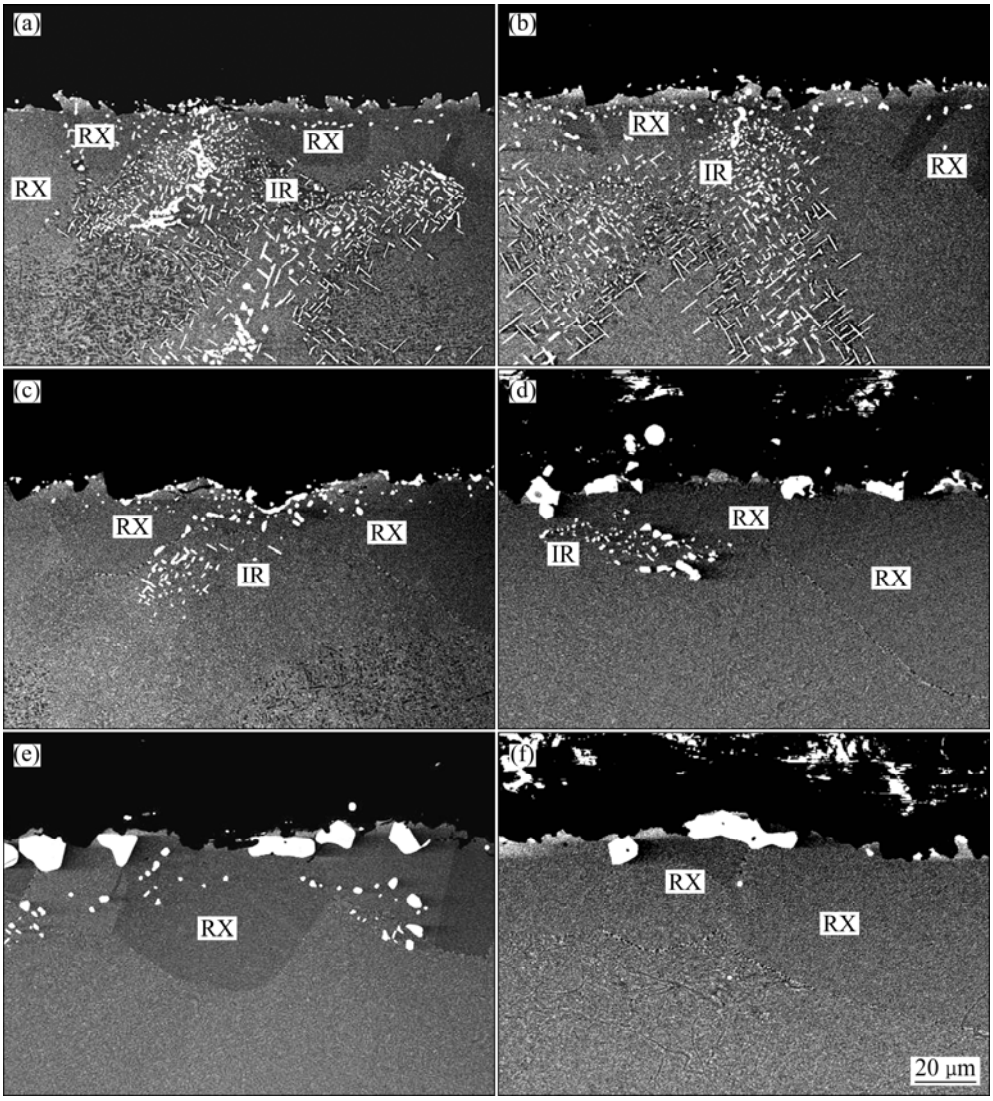

Fig. 4 BSE images showing microstructural morphologies of samples close to grit blasting surface after annealing at 1280 °C for 10 min (a), 30 min (b), 60 min (c), 240 min (d), 600 min (e) and 1200 min (f), respectively

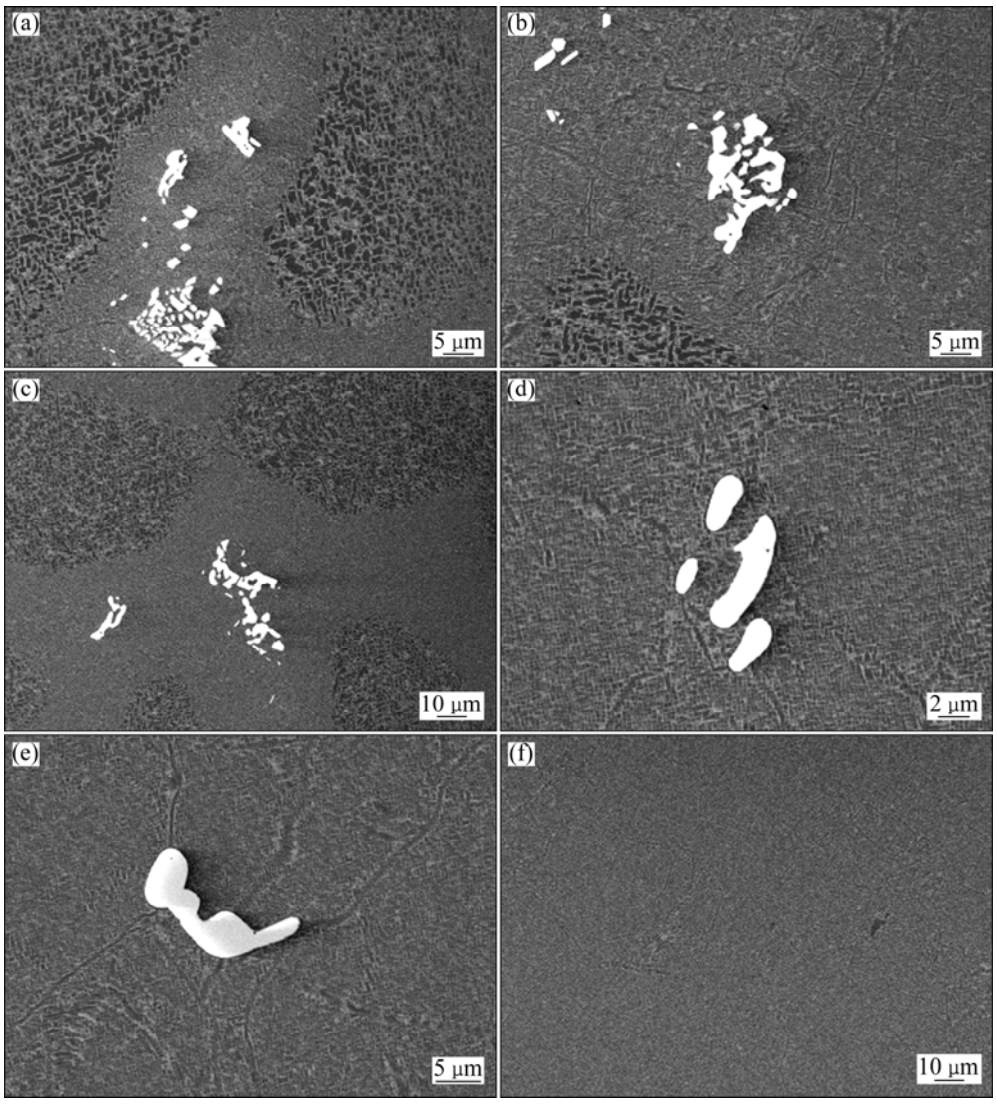

Fig. 5 BSE images showing microstructural morphologies of matrix further away from grit blasting surface after annealing at 1280 °C for 10 min (a), 30 min (b), 60 min (c), 240 min (d), 600 min (e) and 1200 min (f), respectively

Y-NiMo phase. The compositions of other white precipitates were analyzed by EDS. And the results showed that the white precipitates mainly consisted of Ni and Mo with mole ratio nearly 1:1. Furthermore, the white phase was enveloped by γ' phase, as illustrated in Fig. 4(a). Based on the morphology and the chemical content, the precipitates should be Y-NiMo phase [15−17].

Secondly, the reasons accounted for the formation of secondary Y-NiMo precipitates were discussed. It was believed that the secondary Y-NiMo phase formed by the reaction γ-Ni(Mo)→Y-NiMo+γ'-Ni_3Al [17]. For one thing, the element Mo segregated in the interdendritic region seen in Table 1, which means the interdendritic region provided the chemical contents. For another, plastic deformation induced by grit blasting accelerated the reaction and provided the driving force as there was almost no secondary Y-NiMo phase in the matrix far from the grit blasted surface (Fig. 5(a)).

Then, the deep insights about the effect of the plastic deformation were cast. Dislocations and point defects were introduced after plastic deformation. Since the Y-NiMo phase transformation involves the formation of new phases that have a composition and crystal structure different from the parent one, the atomic rearrangements via diffusion were required. Evidently, the diffusion process was time-dependent. The Y-NiMo phase precipitated from the Ni_3Al based alloy IC6E after aging at 1070 °C for 100 h [19]. Except the influence of annealing temperature, atomic migration along dislocations was much faster than through the regular lattice. Thus, no wonder so much Y-NiMo phase precipitated in ten minutes in contrast with the strain-free matrix.

The amount and size of secondary Y-NiMo phase increased with the annealing time, as indicated in Fig. 4(b). The Y-NiMo phase exhibited different shapes both in Figs. 4(a) and (b) with the distance further away from the surface of the sample where the residual stress gradient existed. This can be explained by the stored energy gradient which provided the driving force for the Y-NiMo phase transformation during annealing. Therefore, it can be concluded that the granule Y-NiMo phase transformation needed higher energy than the needlelike one considering the interfacial energy and the strain energy.

In total, the above studies revealed the reasons for the precipitation of the Y-NiMo phase in the interdendritic region. It can be seen that the recrystallization proceeded along with the precipitation of the Y-NiMo phase based on the results discussed earlier of Figs. 4(a) and (b). Namely, precipitation and recrystallization occurred concurrently. The general case of the interaction between precipitation and recrystallization has been mostly studied in the aluminium alloy [20]. HUMPHREYS and HATHERL [20] concluded that the recrystallization behaviour could be divided into three regimes: precipitation before recrystallization, precipitation and recrystallization occurring concurrently and recrystallization before precipitation. Evidently, in the present study it is observed that precipitation and recrystallization occurred concurrently. As a consequence of this, precipitation of Y-NiMo phase would have a profound effect on the recrystallization behaviour which led to the difference in the recrystallization kinetics between the dendrite arm and the interdendritic region.

As mentioned above, nucleation on the defects such as dislocations and vacancies could consume the stored energy which would become less for the driving force of recrystallization. In addition, the presence of Y-NiMo phase would prevent recrystallization process. It can be further explained by microhardness of the Y-NiMo phase. XIAO and HAN pointed out [21] that the Y-NiMo phase was a hard phase whose hardness was nearly three times that of γ' phase. This could also be supported by Fig. 2(a) where it can be seen that the coherent microstructure of γ' particles and γ was more severely distorted than the Y-NiMo phase. Hence, the Y-NiMo phase was not easily dissolved by the advancing front of the recrystallized grains.

When the sample was annealed at 1280 °C for 1 h, the recrystallized grains went on growing inwards into the matrix, as shown in Fig. 4(c). Nevertheless, the amount of Y-NiMo phase reduced greatly in contrast with Figs. 4(a) and (b). HAN et al [17] pointed out that the Y-NiMo phase was metastable and can transform back to the γ-Ni phase. Figure 4(c) indicates that the secondary Y-NiMo phase partially transformed to γ phase. The Y-NiMo phase became less and less but still existed, as shown in Figs. 4(d)−(f), with the annealing time. While the primary Y-NiMo phase completely dissolved back into the matrix with the strain-free area, as illustrated in Fig. 5(f). This difference can be explained by the additional precipitation and dissolution of the Y-NiMo phase in the strain area. It should be noticed that the Y-NiMo phase did not retard the advancing front of the recrystallized grains after 10 h, as shown in Figs. 4(e) and (f). As expected, the recrystallization velocity in the interdendritic region could accelerate when the Y-NiMo phase did not hinder the recrystallization.

3.4 Role of Y-NiMo phase

Considering the Y-NiMo phase segregated only in the interdendritic region, the kinetics of recrystallization in the dendrite arm was considered a reference system to discuss the role of the Y-NiMo phase. In the present work, recrystallization proceeded in the form of a surface layer, so the volume fraction of the recrystallization X_r can be identified as $X_r=R(t)/R_f$, where $R(t)$ was the average recrystallization depth at the time of t and R_f was the average recrystallization depth after infinite annealing time [6], namely, R_f can be considered the recrystallization depth at 1200 min as derived from Fig. 3. The results of the volume fraction of recrystallization are shown in Fig. 6. Then, on the basis of volume fraction in the interdendritic region and dendrite arm, the difference value between the two regions was got as illustrated in the plot and the value can be used to discuss the role of the Y-NiMo phase as just mentioned.

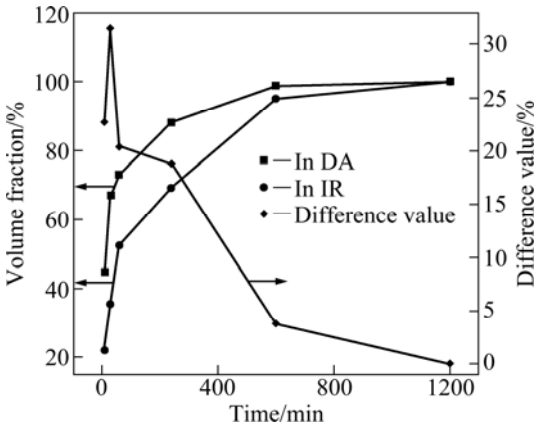

Fig. 6 Volume fraction of recrystallization against annealing time and difference value of volume fraction between dendrite arm and interdendritic region

The difference value firstly increased and then descended as shown in Fig. 6 which agreed with Y-NiMo phase firstly precipitated and became more,

then dissolved back into the matrix. It confirmed the pinning effect of the Y-NiMo phase. Obviously, the first two difference values of recrystallization volume fraction between dendrite arm and interdendritic region were the highest as the Y-NiMo phase precipitated and coarsened, as shown in Figs. 4(a) and (b). In addition, when the Y-NiMo phase did not retard the advancing front of the recrystallized grains after 10 h as shown in Fig. 4(e), the difference value was so small, just about 4%. In conclusion, the Y-NiMo phase inhibited the recrystallization and this effect was weakened as the Y-NiMo phase dissolved. Finally, the Y-NiMo phase did not inhibit the recrystallization; however, depth in the dendrite arm was still deeper than in the interdendritic region, as shown in Figs. 3(b) and (c). In addition to the consumption of stored energy during precipitation, there was another reason accounting for it. The microhardness of the sample in the interdendritic region (HV385.2) was harder than that in the dendrite arm (HV340.8). This was partially due to the presence of the primary Y-NiMo phase. Correspondently, the plastic area during grit blasting in the interdendritic region was not larger than that in the dendrite arm. So, the recrystallization depth was different in the two regions. In brief, the consumption of stored energy and the different microhardness made the recrystallization depth deeper in the dendrite arm than in the interdendritic region.

4 Conclusions

1) Recrystallization kinetics in the dendrite arm was significantly different from that in the interdendritic region. The recrystallization depth and velocity in the dendrite arm were respectively deeper and faster than those in the interdendritic region.

2) The primary Y-NiMo phase dissolved gradually during annealing, while the secondary Y-NiMo phase precipitated in the interdendritic region and coarsened with the annealing time. The secondary Y-NiMo phase dissolved back into the matrix as the annealing time further increased.

3) The Y-NiMo phase had a strong pinning effect on the recrystallization of a Ni_3Al-based superalloy IC21, but this effect would weaken when the Y-NiMo phase dissolved. Eventually, the recrystallized grains did not reach a uniform depth between the dendrite arm and the interdendritic region.

References

[1] MENG J, JIN T, SUN X F, HU Z Q. Effect of surface recrystallization on the creep rupture properties of a nickel-base single crystal superalloy [J]. Materials Science and Engineering A, 2010, 527(23): 6119−6122.

[2] ZHANG B, LIU C K, LU X, TAO C H, JIANG T. Effect of surface recrystallization on the creep rupture property of a single-crystal superalloy [J]. Rare Metals, 2010, 29(4): 413−416.

[3] OKAZAKI M, OHTERA I, HARADA Y. Damage repair in CMSX-4 alloy without fatigue life reduction penalty [J]. Metallurgical and Materials Transactions A, 2004, 35(2): 535−542.

[4] OKAZAKI M, HIURA T, SUZUKI T. Effect of local cellular transformation on fatigue small crack growth in CMSX-4 and CMSX-2 at high temperature [C]//POLLOCK T M, KISSINGER R D, BOWMAN R R, GREEN K A, MCLEAN M, OLSON S L, SCHIRRA J J. Superalloys 2000. Warrendale: TMS, 2000: 505−514.

[5] BÜRGEL R, PORTELLA P D, PREUHS J. Recrystallization in single crystals of nickel base superalloys [C]//POLLOCK T M, KISSINGER R D, BOWMAN R R, GREEN K A, MCLEAN M, OLSON S L, SCHIRRA J J. Superalloys 2000. Warrendale: TMS, 2000: 229−238.

[6] ZHANG B, LIU C K, HE Y H, TAO C H, LU X. Recrystallization of SRR99 single-crystal superalloy: Kinetics and microstructural evolution [J]. Rare Metals, 2010, 29(3): 312−316.

[7] JO C Y, CHO H Y, KIM H M. Effect of recrystallisation on microstructural evolution and mechanical properties of single crystal nickel base superalloy CMSX–2 part 1—Microstructural evolution during recrystallization of single crystal [J]. Materials Science and Technology, 2003, 19(12): 1665−1670.

[8] COX D C, ROEBUCK B, RAE C M F, REED R C. Recrystallisation of single crystal superalloy CMSX-4 [J]. Materials Science and Technology, 2003, 19(4): 440−446.

[9] LI Y N, HAN Y F. Recrystallization of Ni_3Al base single crystal alloy IC6SX with different surface mechanical processes [J]. Journal of Materials Science & Technology, 2010, 26(10): 883−888.

[10] LI Ya-nan, HE Di, LI Shu-suo, HAN Ya-fang. Surface recrystalliztion in a Ni_3Al base single crystal alloy IC6SX [J]. Acta Metallurgica Sinica, 2008, 44(4): 391−396. (in Chinese)

[11] BAKER I, VIENS D V, SCHULSON E M. Annealing studies of cold-rolled Ni_3Al [J]. Journal of Materials Science, 1984, 19: 1799−1804.

[12] LI P, LI S S, HAN Y F. Influence of solution heat treatment on microstructure and stress rupture properties of a Ni_3Al base single crystal superalloy IC6SX [J]. Intermetallics, 2011, 19(2): 182−186.

[13] JIANG Li-wu, LI Shu-suo, QIU Zi-cheng, HAN Ya-fang. Effects of withdrawal rate on microstructure and stress rupture properties of a Ni_3Al-based single crystal superalloy IC6SX [J]. Acta Metallurgica Sinica, 2009, 45(5): 547−552. (in Chinese)

[14] DING R G, OJO O A, CHATURVEDI M C. Laser beam weld-metal microstructure in a yttrium modified directionally solidified Ni_3Al-base alloy [J]. Intermetallics, 2007, 15(12): 1504−1510.

[15] XIAO C B, HAN Y F. Study of precipitates due to the addition of silicon in yttrium modified Ni−Al−Mo−B alloy IC6 [J]. Materials Science and Engineering A, 2002, 323(1−2): 58−61.

[16] SONG Jin-xia, XIAO Cheng-bo, LI Shu-suo, HAN Ya-fang. Effect of long term aging on microstructure and mechanical properites of Ni_3Al base alloy IC6 [J]. Acta Metallurgica Sinica, 2002, 38(3): 250−254. (in Chinese)

[17] HAN Y F, LI S H, JIN Y, CHATURVEDI M C. Effect of 900−1150 °C aging on the microstructure and mechanical properties of a DS casting Ni_3Al-base alloy IC6 [J]. Materials Science and Engineering A, 1995, 192−193: 899−907.

[18] BOND S D, MARTIN J W. Surface recrystallization in a single crystal nickel-based superalloy [J]. Journal of Materials Science, 1984, 19: 3867−3872.

[19] LI M, SONG J X, LI S S, HAN Y F. Effects of long-term aging at

1070 °C on microstructure and mechanical properties of Ni_3Al-base alloy IC6E [J]. Materials Science Forum, 2010, 650: 205−209.

[20] HUMPHREYS F J, HATHERLY M. Recrystallization and related annealing phenomena [M]. 2nd ed. New York: Elsevier, 2004: 48−65.

[21] XIAO C B, HAN Y F. Effect of silicon on microstructure and stress rupture properties at 1100 °C of yttrium modified Ni−Al−Mo−B alloy IC6 [J]. Journal of Materials Science, 2001, 36(4): 1027−1030.

一种 Ni_3Al 基单晶高温合金的再结晶动力学及组织变化

武雨潇[1], 张 恒[1], 李福林[1], 李树索[1,2], 宫声凯[1,2], 韩雅芳[1,3]

1. 北京航空航天大学 材料科学与工程学院，北京 100191；
2. 北京航空航天大学 空天先进材料与服役教育部重点实验室，北京 100191；
3. 北京航空材料研究院，北京 100095

摘 要：研究了一种 Ni_3Al 基单晶高温合金的再结晶动力学及组织变化，解释了造成枝晶干和枝晶间再结晶行为不一致的原因。 单晶合金经表面喷砂处理，再在惰性气氛中，于 1280 °C 下退火不同时间形成再结晶晶粒。研究发现：枝晶干再结晶层厚度大于枝晶间再结晶厚度，枝晶干再结晶速率快于枝晶间再结晶速率。在退火过程中，枝晶间有 Y-NiMo 相析出，且强烈抑制再结晶。然而，随着时间的延长 Y-NiMo 析出相逐渐溶解，且抑制再结晶的作用逐渐减弱，最终，枝晶干再结晶层厚度仍然大于枝晶间再结晶厚度。

关键词：再结晶；动力学；Y-NiMo 相；Ni_3Al 基单晶高温合金

(Edited by YANG Hua)